Synthesis of hexagonal lanthanum germanate apatites through site selective isovalent doping with yttrium

E. Kendrick and P.R. Slater*

Chemistry, University of Surrey, Guildford, Surrey. GU2 7XH, UK

*Correspondence to:

Dr. P.R. Slater

Materials Chemistry Group, Chemistry, SBMS, University of Surrey, Guildford, Surrey. GU2 7XH. UK

Tel. +44 (0)1483 686847

Fax +44 (0)1483 686851

p.slater@surrey.ac.uk

Abstract

Apatite-type lanthanum silicates/germanates have been attracting considerable interest as a new class of oxide ion conductors, whose conductivity is mediated by oxide ion interstititials. For the germanates, it has been shown that, depending on composition, the cell can be either hexagonal or triclinic, with evidence for reduced low temperature conductivities for the latter, attributed to increased defect trapping in this lower symmetry cell. In this paper we show that site selective doping of Y into the triclinic apatite-type oxide ion conductors, $La_{9.33+z}(GeO_4)_6O_{2+3z/2}$ ($0.33 \leq z \leq 0.67$) results in a hexagonal lattice for the complete series with correspondingly enhanced low temperature conductivity.

Keywords: A Oxides, B. Chemical Synthesis, C. X-ray diffraction, D. Ionic Conductivity.

Introduction

Apatite materials have attracted considerable interest for a range of applications, including electrolytes for solid oxide fuel cells (SOFCs), bioceramics for bone implants, and hazardous waste encapsulation materials. In terms of the former it is the Lanthanum silicate and germanate materials, $La_{9.33+z}(Si/GeO_4)_6O_{2+3z/2}$ which have attracted considerable attention due to their high oxide ion conductivities at elevated temperatures [1-17]. In contrast to the traditional fluorite and perovskite-type oxide ion conductors, where conductivity is mediated by oxide ion vacancies, the weight of experimental and theoretical evidence for the apatite systems indicates that they conduct via an interstitial mechanism. Consequently high conductivity is favoured by the presence of oxygen interstitials, which can be either present as oxygen hyperstoichiometry ($z>0$) or Frenkel defects [4,9,10,12,13].

So far, the majority of the work on these apatite systems have focused on the silicate systems, which can be partly related to the additional complexities shown by the apatite germanates. In particular, the germanates are complicated by the change in the crystal symmetry from hexagonal to triclinic as the La content/oxygen content increases. In this respect Leon-Reina *et al.* have reported the preparation of single phase samples of $La_{9.33+z}(GeO_4)_6O_{2+3z/2}$ for $0.19\leq z\leq 0.42$, with samples in the range $0.19\leq z\leq 0.27$ possessing hexagonal symmetry, while samples with higher La content, $0.33\leq z\leq 0.42$, exhibit a triclinic cell [6]. In terms of potential applications the triclinic cell is not ideal, as it results in lower oxide ion conductivities at low temperatures, most likely due to enhanced defect trapping in the lower symmetry cell.

The origin of the triclinic distortion in apatite materials has been discussed in detail by Baikie *et al*., where the authors have described the structure of apatite-type materials

($A_{10}(MO_4)_6X_2$; A=alkaline earth, rare earth, Pb; M=Si, Ge, P, V; X=O, OH, Halides) in terms of a "microporous" framework ($A(1)_4(MO_4)_6$) composed of face sharing $A(1)O_6$ trigonal meta-prismatic columns, that are corner connected to the MO_4 tetrahedra (figure 1) [17]. This framework allows some flexibility to accommodate the remaining $A(2)_6X_2$ units. A triclinic apatite cell is obtained in systems such as the lanthanum germanates due to the large size of the $A(1)_4(MO_4)_6$ framework. This places extension stress at the A cation site in the $A(2)_6X_2$ unit, and compression stress at the M site, which are relieved by the MO_4 tetrahedra tilting in the triclinic cell. The presence of interstitial oxygen atoms also enhances triclinic distortion, most probably by contributing to a further expansion of the $A(1)_4(MO_4)_6$ framework, hence accounting for the fact that samples with low oxygen excess ($z \leq 0.27$) are hexagonal, whereas higher oxygen content samples are triclinic [6]

The ideal way to overcome this structural stress would be to increase the size of the A(2) cations. Thus $Ca_{10}V_6O_{24}F_2$ is triclinic, while isovalent doping with the larger Pb cation results in hexagonal symmetry [17]. However, such an isovalent doping strategy is not possible for $La_{9.33+z}(GeO_4)_6O_{2+3z/2}$, as La is the largest lanthanide. Therefore, we have investigated an alternative approach, namely the doping of a smaller rare earth, Y, into $La_{9.33+z}(GeO_4)_6O_{2+3z/2}$, with the aim of selectively substituting for the La site in the $A(1)_4(MO_4)_6$ framework in order to relieve strain by reducing the size of this framework. Atomistic modelling studies of the related apatite lanthanum silicates have predicted a preference for Y substitution in the $A(1)_4(MO_4)_6$ framework [18]. In this paper we confirm that such site selective doping is successful, and does indeed lead to the formation of hexagonal apatites even for high oxygen contents.

Experimental

Samples, $La_{9.33+z-x}Y_x(GeO_4)_6O_{2+3z/2}$ ($0 \leq z \leq 0.67$; x=1, 2, 3), were prepared from high purity La_2O_3, Y_2O_3 and GeO_2. The dried powders were intimately mixed in the correct ratios and heated to 1100°C for 24 hours with an intermediate regrind. Phase purity was established through X-ray powder diffraction (Panalytical X'Pert Pro diffractometer, Cu $K\alpha_1$ radiation). For preliminary structural studies to determine the location of the Y dopant, data were collected over 12 hours in the range 10-120° (2θ). Rietveld analysis was then performed using the GSAS suite of programs, with the fits compared for Y on each of the La sites [19].

Pellets (1.6 cm diameter) for conductivity measurements were prepared as follows: the powders were ball milled (350 rpm, Fritsch Pulverisette 7 Planetary Mill) for 1 hour before pressing at 8000 kg cm^{-2}. The pressed pellets were then heated at 1300°C for 2 hours, leading to densities > 85% theoretical. Both sides of the pellet were coated with Au paste and then heated to 700°C for 1 hour to ensure bonding to the pellet. Conductivity measurements were made in air using AC impedance spectroscopy (Hewlett Packard 4182A impedance analyser).

Results and discussion

X-ray diffraction indicated that single phase samples of $La_{9.33+z-x}Y_x(GeO_4)_6O_{2+3z/2}$ were formed for $0.22 \leq z \leq 0.67$ (y=1, 2, 3), representing a larger solid solution range compared to that reported by Leon-Reina *et al.* for the undoped system ($0.19 \leq z \leq 0.42$) [6]. Contrary to samples without Y doping, where a hexagonal lattice is obtained for $0.19 \leq z \leq 0.27$, with triclinic samples observed for higher values of z, all Y doped compositions ($0.22 \leq z \leq 0.67$) were shown to be hexagonal (figure 2).

In order to determine the location of the Y dopant, preliminary refinement of X-ray diffraction data was performed for a range of samples. In all cases the R factors were lowest for Y located in the A cation site within the $A(1)_4(MO_4)_6$ framework (e.g. $La_8Y_2(GeO_4)_6O_3$; Chi^2 = 2.83 (Y on A(1) site), 4.67 (Y on A(2) site). Thus in agreement with the predicted strategy, selective doping of Y in the $A(1)_4(MO_4)_6$ framework stabilises the hexagonal lattice. Due to the general insensitivity of X-rays to light atoms, such as oxygen, and the considerable structural distortion around the interstitial site, further more detailed neutron diffraction studies are planned to structurally characterise these systems fully, particularly to elucidate the oxygen interstitial sites.

Refinement of the cell parameters shows that the Y doping leads to an overall reduction in unit cell size as expected due to the smaller size of Y^{3+} compared to La^{3+}, with the cell parameters obeying Vegard's law, consistent with Y substitution on the same site across the series. However, this contraction is not uniform in all directions, with the main contraction along the c axis. This can be most clearly visualised by plotting the % change along each of the unit cell axes with increasing Y content (figure 3). Further increases in Y content are also possible, i.e. x>3, however peak broadening indicative of a return to the triclinic cell is observed for these higher Y dopant levels.

High oxide ion conductivities were observed for all samples (0.025-0.040 Scm^{-1} at 800°C). Compared to triclinic $La_{9.33+z}(GeO_4)_6O_{2+3z/2}$ samples without Y doping, the conductivities were enhanced at lower temperatures, while at higher temperatures they are comparable (figure 4). The convergence of the data at higher temperatures (>700°C) can be related to the fact that in this temperature range, even the undoped $La_{9.33+z}(GeO_4)_6O_{2+3z/2}$ samples are hexagonal; prior reports showing that there is a change from a triclinic to a hexagonal cell at high temperatures [7,16]. Thus the

enhanced lower temperature conductivity can be correlated with the more facile oxide ion conduction within the higher symmetry hexagonal lattice.

Conclusions

In summary, we have shown that site selective doping of $La_{9.33+z}(GeO_4)_6O_{2+3z/2}$ with a smaller rare earth, Y, leads to a stabilisation of the hexagonal lattice, even for high oxygen contents. Furthermore this has the effect of enhancing the low temperature conductivities.

References

1. S. Nakayama, H. Aono, Y. Sadaoka, Chem. Lett. (1995) 431.

2. S. Nakayama, M. Sakamoto, M. Higuchi, K. Kodaira, J. Mater. Sci. Lett. 19 (2000) 91.

3. S. Tao, J.T.S. Irvine, Mater. Res. Bull. 36 (2001) 1245.

4. J.E.H. Sansom, D. Richings, P.R. Slater, Solid State Ionics 139 (2001) 205.

5. H. Arikawa, H. Nishiguchi, T. Ishihara, Y. Takita, Solid State Ionics 136-137 (2000) 31.

6. L. Leon-Reina, M.E. Martin-Sedeno, E.R. Losilla, A. Caberza, M. Martinez-Lara, S. Bruque, F.M.B. Marques, D.V. Sheptvakov, M.A.G. Aranda; Chem. Mater. 15 (2003) 2099.

7. E.J. Abram, C.A. Kirk, D.C. Sinclair, A.R. West; Solid State Ionics 176 (2005) 1941.

8. J.E.H. Sansom, L. Hildebrandt, P.R. Slater, Ionics 8 (2002) 155.

9. J.R. Tolchard, M.S. Islam, P.R. Slater; J. Mater. Chem. 13 (2003) 1956.

10. L. Leon-Reina, E.R. Losilla, M. Martinez-Lara, M.C. Martin-Sedeno, S. Bruque, P.Nunez, D.V. Sheptyakov, M.A.G. Aranda; Chem. Mater. 17 (2005) 596.

11. V.V. Kharton, A.L. Shaula, M.V. Patrakeev, J.C. Waerenborgh, D.P. Rojas, N.P. Vyshatko, E.V. Tsipis, A.A. Yaremchenko, F.M.B. Marques; J. Electrochem. Soc. 151 (2004) A1236.

12. J.E.H. Sansom, J.R. Tolchard, D. Apperley, M.S. Islam, P.R. Slater; J. Mater. Chem. 16 (2006) 1410.

13. E. Kendrick, M.S. Islam, P.R. Slater; *J. Mater. Chem*. 2007, DOI:10.1039/B704426G

14. Y. Masubuchi, M. Higuchi, S. Kikkawa, K. Kodaira, S. Nakayama; Solid State Ionics 175 (2004) 357.

15. S. Celerier, C. Laberty-Robert, J.W. Long, K.A. Pettigrew, R.M. Stroud, D.R. Rolison, F. Ansart, P. Stevens, Adv. Mater. 18 (2006) 615.

16. L. Leon-Reina, J.M. Porras-Vasquez, E.R. Losilla, M.A.G. Aranda; J. Solid State Chem. 180 (2007) 1250.

17. T. Baikie, P.H.J. Mercier, M.M. Elcombe, J.Y. Kim, Y. Le Page, L.D. Mitchell, T.J. White, P.S. Whitfield; Acta Crystallographica B 63 (2007) 251.

18. J. R. Tolchard, P. R. Slater and M. S. Islam; Adv. Funct. Mater. (2007) DOI 10.1012/adfm.200600789.

19. A.C. Larson, R.B. Von Dreele. Los Alamos National Laboratory, Report. No LA-UR-86-748, 1987.

Figure Legends

Figure 1(a) Illustration of the "microporous" $A(1)_4(MO_4)_6$ framework of the apatite ($A_{10}(MO_4)_6X_2$) structure (tetrahedra=MO_4; A(1) cations at centre of trigonal meta-prisms). The remaining $A(2)_6X_2$ units occupy the cavities within this framework. (b) Illustration of the structure as a whole (Large White Spheres= A2 cations, Small White Spheres= X anions).

Figure 2. X-ray diffraction patterns for $La_{9.83}(GeO_4)_6O_{2.75}$ and $La_8Y_2(GeO_4)_6O_3$.

Figure 3. Plot of % change in cell parameters and cell volume with increasing Y content for $La_{9.55-x}Y_x(GeO_4)_6O_{2.33}$.

Figure 4. Conductivity plots for $La_{9.83}(GeO_4)_6O_{2.75}$ (▲), $La_{7.83}Y_2(GeO_4)_6O_{2.75}$ (●), and $La_8Y_2(GeO_4)_6O_3$ (■)

Figure 1a

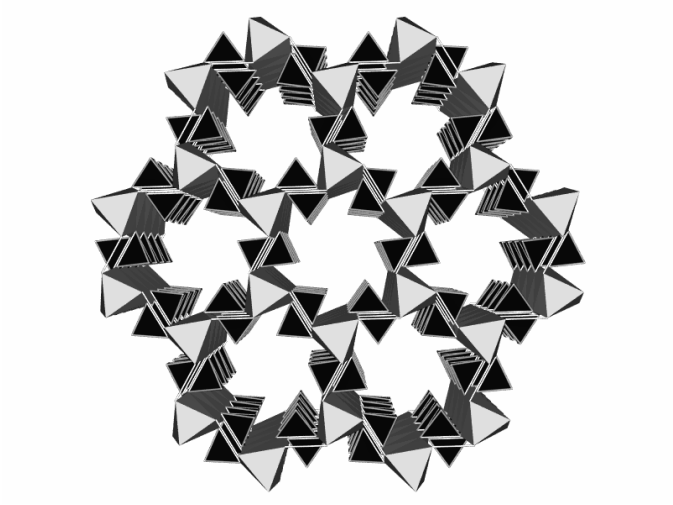

Figure 1b

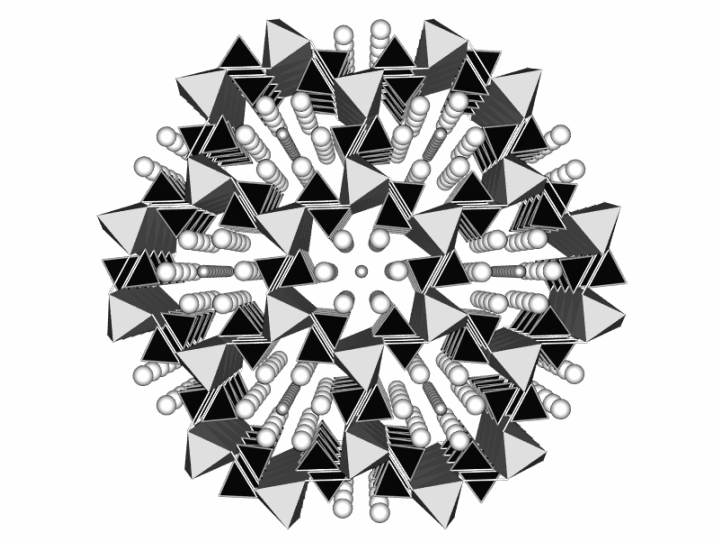

Figure 2

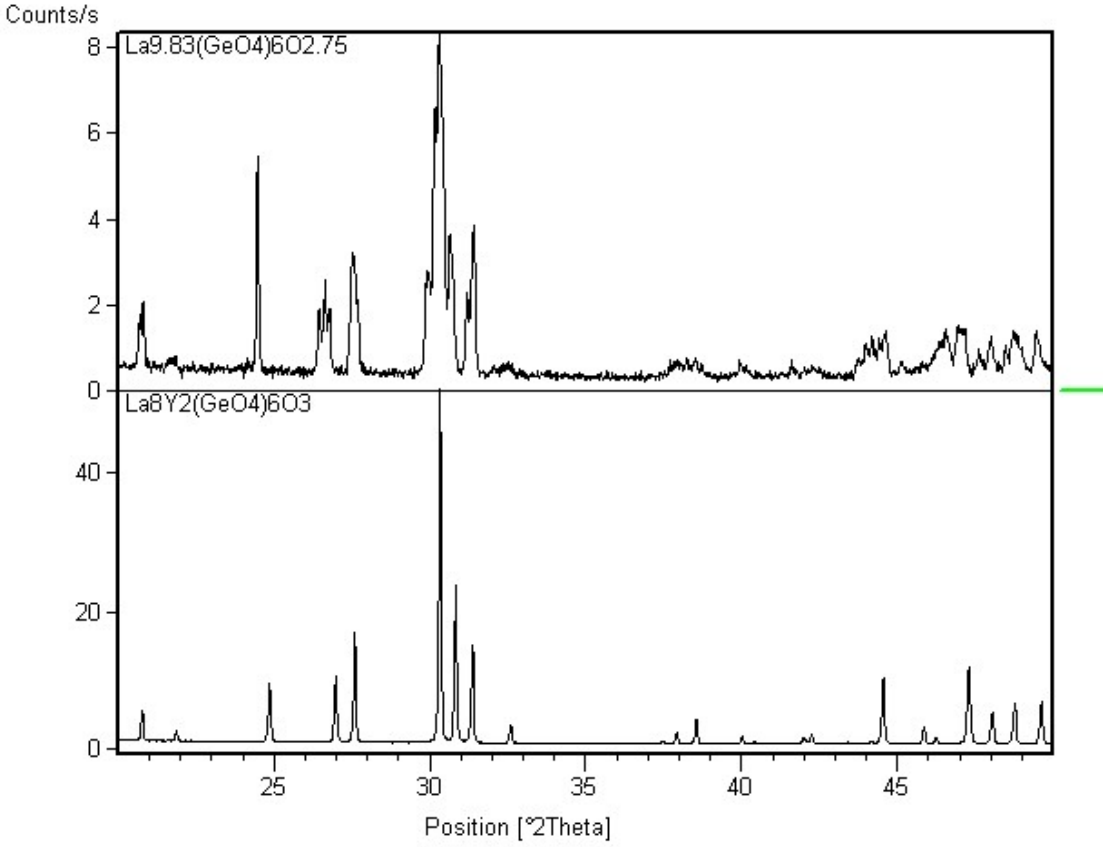
Counts/s
La9.83(GeO4)6O2.75
La8Y2(GeO4)6O3
8
6
4
2
0
40
20
0
25
30
35
40
45
Position [°2Theta]

Figure 3

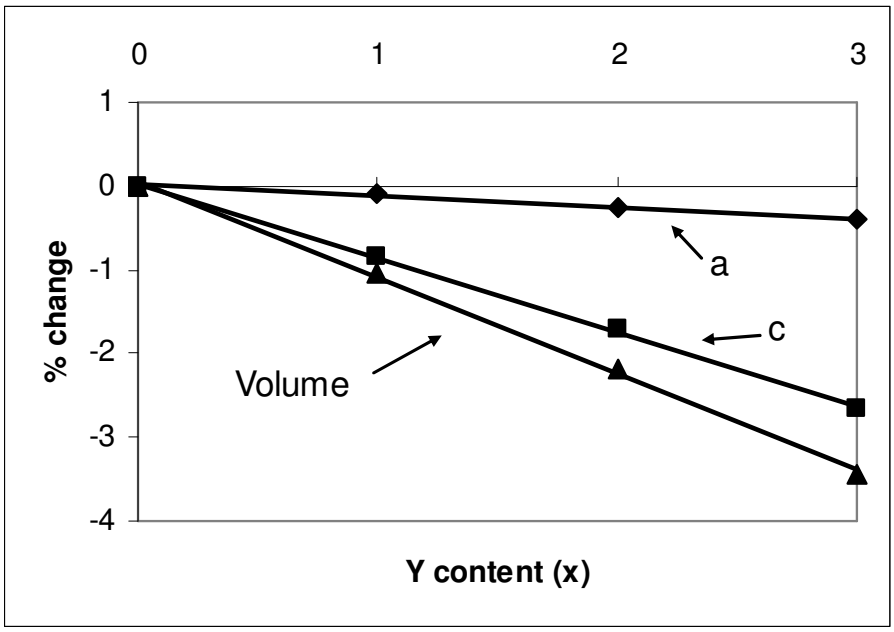

Figure 4